Electronic Supplementary Material (ESI) for Journal of Materials Chemistry C.

Nonstoichiometry, Structure, and Properties in $Ba_{1-x}TiO_3$ Thin Films

Arvind Dasgupta,[1,2] Sahar Saremi,[1] Ruijuan Xu,[1] Liv Dedon,[1,2] Shishir Pandya,[1] Anoop R. Damodaran,[1] Lane W. Martin[1,2]

[1] Department of Materials Science and Engineering, University of California, Berkeley, Berkeley, CA 94720

[2] Materials Sciences Division, Lawrence Berkeley National Laboratory, Berkeley, CA 94720

Supplementary Information

1. Fitting the Oxygen Resonance Curve in Rutherford Backscattering Spectrometry

During a Rutherford backscattering spectrometry (RBS) studies, He^{2+} ions incident at 3.040 MeV undergo increased scattering from the oxygen lattice due to a resonant phenomenon.[1] The reaction $^{16}O\ (\alpha,\alpha)\ ^{16}O$ has to therefore be modelled by non-Rutherfordian cross sections which are larger than conventional cross sections and this can allow for a quantification of the anions concentration present in our lattice. For this purpose, cross-section parameters for a geometry and energy range similar to our experiment previously reported in literature were used.[2] A methodology which has been described elsewhere[3] was followed to ensure a reliable and good fit of the experimental data. It has to be noted that the fits are very sensitive to a wide variety of input parameters, and there is some error associated with the cross section parameters the scattering angles themselves. Therefore, the error associated with the anion chemistry fits (~3%) is larger than the error associated with the cation chemistry fits (~1-2%). In this work, we are more interested in the trends of anion chemistry rather than the exact numbers themselves

2. X-ray Diffraction

X-ray diffraction line scans of all the heterostructures showed the existence of single-phase, epitaxial films. The existence of Laue fringes about the 001_{PC}-diffraction condition during the X-ray diffraction line scans (Figures S1a-c) is evidence of the quality of the thin films as well as the presence of pristine surfaces and interfaces.[4] Also, in order to further investigate the relative crystalline quality of the thin films, X-ray rocking curves were measured about the 002_{PC}-diffraction condition for the film and the substrate (Figures S1d-f). By comparing the ratios of the full-width-at-half-maximum (FWHM) $\frac{\Delta\omega_{film}}{\Delta\omega_{substrate}}$ we can compare the relative crystallinity of the three heterostructure variants.[5] It is seen that this fraction does not vary much, changing from 2.33 for the heterostructures grown at 1.25 J/cm^2, to 5.15 for the heterostructures grown at 1.45 J/cm^2, to 4.89 for the heterostructures grown at 1.65 J/cm^2. This indicates that the film and the substrates have comparable crystalline quality and there is no significant degradation in crystallinity as we vary the laser fluence.

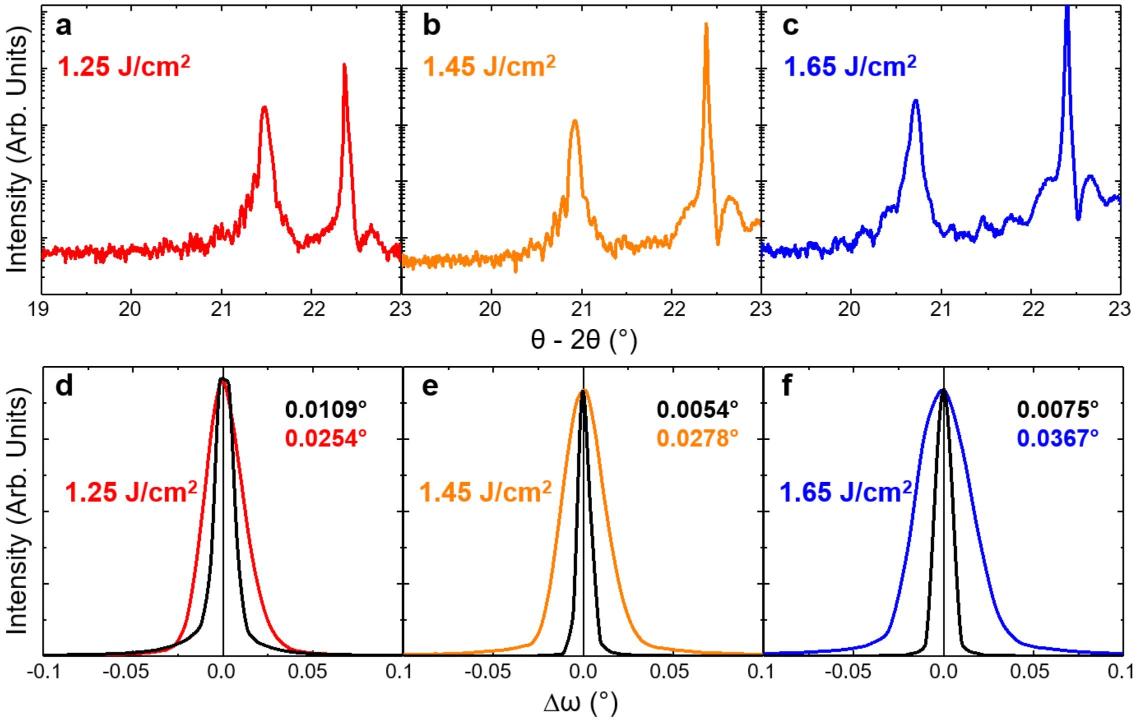

Fig. S1 Close-up of the 2θ-ω X-ray diffraction scans about the 001_{PC}-diffraction condition for the $Ba_{1-x}TiO_y$ films grown at (a) 1.25 J/cm^2, (b) 1.45 J/cm^2, and (c) 1.65 J/cm^2. X-Ray rocking curves about the 002_{PC}-diffraction condition of the heterostructures grown at (d) 1.25 J/cm^2, (e) 1.45 J/cm^2, and (f) 1.65 J/cm^2 with the corresponding full-width-at-half-maximum for the substrate and film.

3. First-order Reversal Curves (FORC)

Hysteresis in any material can be modeled assuming a statistical distribution of hysterons (a bistable unit having a coercive and built in field).[6] In order to determine this statistical distribution, FORC measurements were applied.[7] FORC measurements are completed by performing a number of minor hysteresis loops always starting from a fixed negative field ($E_{sat.}$) with saturated polarization to an increasing maximum field (E_r) (Figures S2a-c). The value of E_r is stepped-up until the loop is completely saturated in the opposite direction. Next, a transform $\rho(E_r, E) = \frac{1}{2}\frac{\partial^2 \mathrm{P}(E_r, E)}{\partial E_r\, \partial E}$ is applied in order to extract the statistical distribution of hysterons in the material.[8] A contour plot of this distribution (main text, Figure 3), helps in visualizing the hysteron distribution in coercive field-internal bias field space.

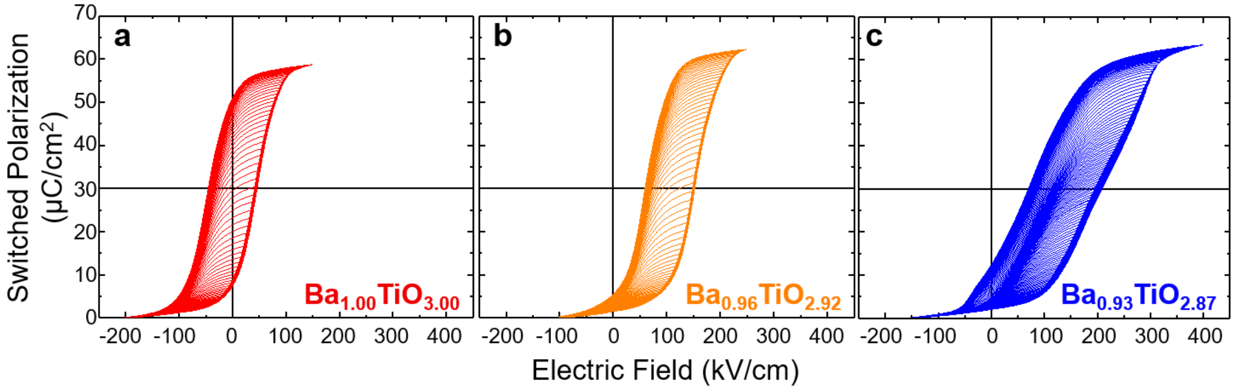

Fig. S2 First-order reversal curve (FORC) studies for (a) $Ba_{1.00}TiO_3$, (b) $Ba_{0.96}TiO_{2.92}$, and (c) $Ba_{0.92}TiO_{2.87}$ heterostructures.

4. Current-Voltage (I-V) Measurements

Leakage in dielectric films can occur due to a number of mechanisms, therefore I-V curves were fit to a number of possible (common) mechanisms in order to determine the likely dominant mechanism. The first, and simplest, mechanism is Ohmic conduction, where current density J is directly proportional to the applied electric field E.[9] In this case, a plot of $\frac{\mathrm{d}\,(\ln J)}{\mathrm{d}\,(\ln E)}$ should be equal to 1. Such analysis (Figure S3a), however, reveals that the actual value is much lower, thereby ruling out this mechanism.

The next potential mechanism to be considered was space-charge-limited conduction, in which conduction is limited by the movement of bulk space charge within the films after being injected freely by ohmic contacts.[9] In this case, the leakage current J is given by $J=\frac{9\mu\varepsilon_0\varepsilon_\mathrm{r}E^2}{8\mathrm{d}}$ where μ is carrier mobility, ε_0 is the permittivity of free space, ε_r is the optical dielectric constant, and d is the film thickness. Therefore, the value of $\frac{\mathrm{d}\,(\ln J)}{\mathrm{d}\,(\ln E)}$ should be equal to 2 in this case and can again be ruled out for the samples as seen (Figure S3a).

The next potential mechanism that was considered was Schottky emission. In this case, the leakage characteristics are dominated by the Schottky contacts formed with the dielectric film,[9] and the leakage current is given by $J=\mathrm{AT}^2\exp\left[-\frac{\varphi_\mathrm{S}}{\mathrm{k_BT}}+\frac{1}{\mathrm{k_BT}}\left(\frac{\mathrm{q}^3E}{4\pi\varepsilon_0\varepsilon_\mathrm{r}}\right)^{\frac{1}{2}}\right]$, where A is the Richardson coefficient, T is the temperature, φ_S is the Schottky barrier height, $\mathrm{k_B}$ is the Boltzmann constant, and q is the charge of an electron. In order to make the equation more tractable, it is often rearranged and a semilog plot of $\frac{J}{\mathrm{T}^2}$ vs. $E^{\frac{1}{2}}$ is constructed. If Schottky emission is dominant, this plot should be linear and the slope of the plot is used to extract the value of ε_r, the optical dielectric constant of the material. As seen here (Figure S3b), however, even though it does have a linear fit, the actual values of optical dielectric constant extracted for the three films (8.96, 9.11, 9.38) are much higher than the literature reported value of 5.9 for $\mathrm{BaTiO_3}$.[10] Therefore, this mechanism is also likely ruled out of consideration.

The final mechanism that was considered was Poole-Frenkel emission. In Poole-Frenkel emission, leakage occurs via a charge trapping/detrapping mechanism, and traps present in the film control the leakage properties.[9] In this case, the leakage in the films is governed by the equation, $J=\mathrm{q}\mu\mathrm{N_C}E\,\exp\left[\frac{-\mathrm{q}(\varphi_\mathrm{T}-\sqrt{\frac{\mathrm{q}E}{\pi\varepsilon_0\varepsilon_\mathrm{r}}}}{\mathrm{rk_BT}}\right]$, where φ_T is the trap energy and r is a scaling constant such that 1 ≤ r ≤ 2. Therefore, in this case, a graph of $\ln\left(\frac{J}{E}\right)$ vs. $E^{\frac{1}{2}}$ should be linear and this is

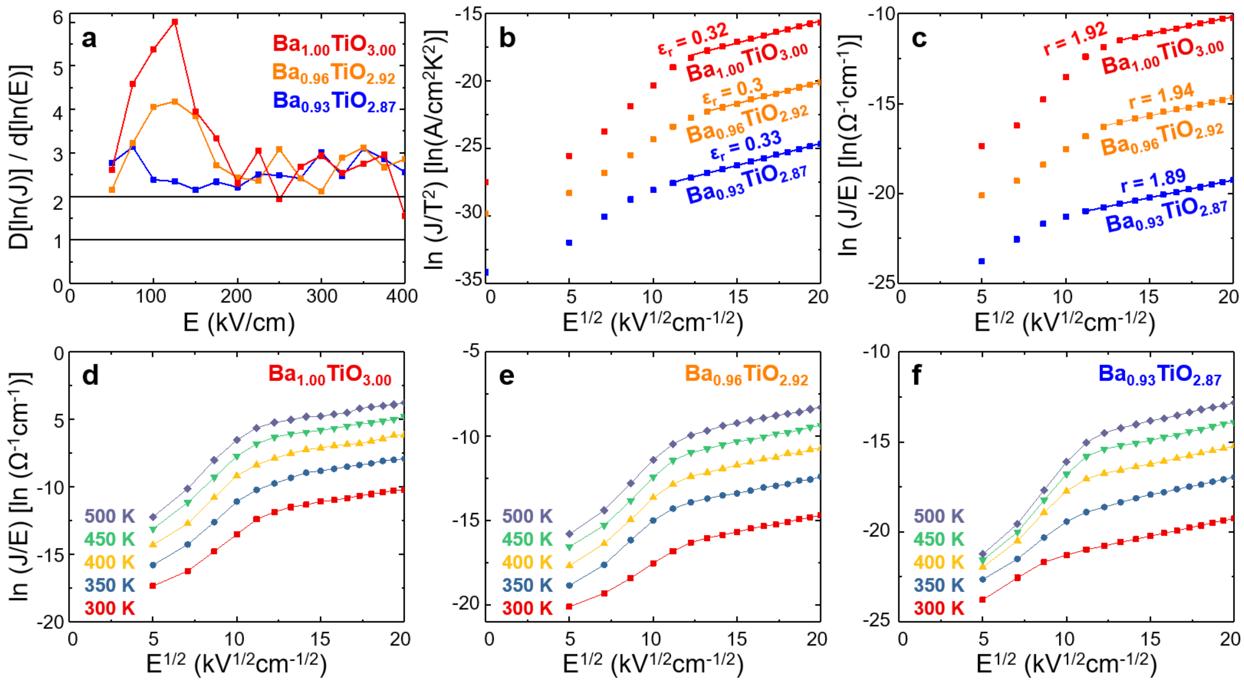

Fig. S3 (a) Plot of $\frac{\mathrm{d}\,(\ln J)}{\mathrm{d}\,(\ln E)}$ as a function of electric field (E) exploring the fit of the data to standard mechanisms including Ohmic (=1) and space-charge-limited conduction (=2). Neither is a good fit for the data. (b) Exploration of data considering Schottky emission as the dominant leakage mechanism reveals a poor match with the expected optical dielectric constant for the material indicating this is not the dominant transport mechanism. (c) Exploration of the data considering Poole-Frenkel emission as the dominant leakage mechanism reveals a good match and thus this is expected to be the dominant effect in operation. Temperature-dependent I-V data for (d) $Ba_{1.00}TiO_3$, (e) $Ba_{0.96}TiO_{2.92}$, and (f) $Ba_{0.93}TiO_{2.87}$ heterostructures.

found to be the case (Figure S3c). In this case, the optical dielectric constant is fixed at 5.9 and the value of r is changed in order to obtain a fit. It can be seen from the graphs that it tends to be linear at high values of electric field, *E*. Since this model provides the most reasonable fit for the leakage current, it was hypothesized that the leakage in our films was indeed occurring through the Poole-Frenkel emission mechanism. In order to extract trap energies, Arrhenius-type fits of the plots of ln *J* vs. 1000/T were used (main text, Figure 4a; raw data Figures S3d-f). It was observed that in all cases, the leakage was governed by a trap with energy $\varphi_T \approx 0.4$ eV.

5. Deep-level Transient Spectroscopy (DLTS)

DLTS is a transient capacitance technique which enables us to probe trap energies and is frequently used for semiconductors. It involves applying a pulse voltage in order to perturb the depletion region in a Schottky junction. The capacitance change of this region is monitored as it relaxes to equilibrium. The boxcar method was used to extract trap energies. This method involves defining a time window consisting of two times t_1 and t_2 between which the change in capacitance will be monitored [$C(t_1)-C(t_2)$]. The emission rate from the trap for this chosen time window when $C(t_1)-C(t_2)$ has a maximum at a temperature T_M is given by $\mathrm{e}(\mathrm{T_M}) = \frac{\mathrm{t_2-t_1}}{\ln\left(\frac{\mathrm{t_2}}{\mathrm{t_1}}\right)}$.

This emission rate varies with the peak temperature T_M as $\mathrm{e}(\mathrm{T_M}) = \gamma\sigma T_M^2 \exp\left(\frac{-E_d}{kT_M}\right)$ where E_d is trap activation energy, γ is a pre-exponential factor and σ is trap capture cross-section Therefore, a plot of $\ln(T_M^2/e(T_M))$ vs. $1000/T_M$ will be linear and the slope can be used to extract trap energies (Figure S4). No clearly discernible peaks were observed for the sample with no barium/oxygen deficiency as well as the sample after barium reintroduction and therefore DLTS fitting was not attempted.

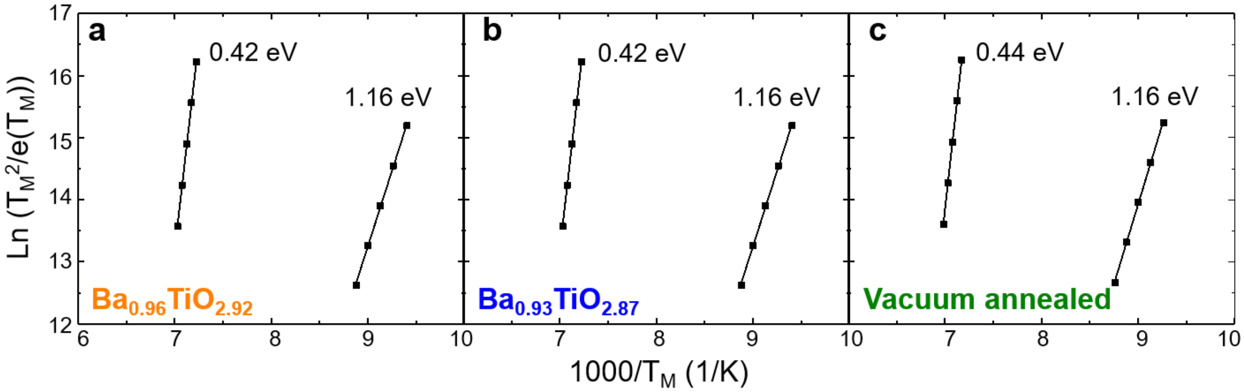

Fig. S4 DLTS fits used to extract trap energies in the (a) $Ba_{0.96}TiO_{2.92}$, (b) $Ba_{0.93}TiO_{2.87}$, and (c) vacuum-annealed $Ba_{0.93}TiO_{2.87}$ heterostructures.

References

[1] J. R. MacDonald, J. A. Davies, T. E. Jackman and L. C. Feldman, *J. Appl. Phys.*, 1983, **54**, 1800-1803.

[2] C. Huan-sheng, S. Hao, T. Jiayong and Y. Fujia, *Nucl. Instrum. Methods Phys. Res. Sect. B Beam Interact. Mater. At.*, 1993, **83**, 449-453.

[3] L. R. Dedon, S. Saremi, Z. Chen, A. R. Damodaran, B. A. Apgar, R. Gao, and L. W. Martin, *Chem. Mater.*, 2016, **28**, 5952-5961.

[4] J. R. Patel and N. Kato, *J. Appl. Phys.*, 1973, **44**, 971-977.

[5] T. Mitsunaga, *The Rigaku J.*, 2009, **25**, 7-12.

[6] I. Mayergoyz, *IEEE Trans. Magn.* 1986, **22**, 603-608.

[7] C. R. Pike, *Phys. Rev. B*, 2003, **68**, 104424.

[8] A. P. Roberts, C. R. Pike and K. L. Verosub, *J. Geophys. Res. Solid Earth*, 2000, **105**, 28461-28475.

[9] F.-C. Chiu, *Adv. Mat. Sc. Eng.*, 2014**,** 2014, 578168.

[10] S. H. Wemple, M. Didomenico and I. Camlibel, *J. Phys. Chem. Solids*, 1968, **29**, 1797-1803.